International Journal of Nanomedicine

Dovepress
open access to scientific and medical research

Open Access Full Text Article

ORIGINAL RESEARCH

Design, characterization, and aerosolization of organic solution advanced spray-dried moxifloxacin and ofloxacin dipalmitoylphosphatidylcholine (DPPC) microparticulate/nanoparticulate powders for pulmonary inhalation aerosol delivery

This article was published in the following Dove Press journal:
International Journal of Nanomedicine
16 September 2013
Number of times this article has been viewed

Jinghua Duan[1,2]
Frederick G Vogt[3]
Xiaojian Li[1]
Don Hayes Jr[4,5]
Heidi M Mansour[6]

[1]University of Kentucky College of Pharmacy, Department of Pharmaceutical Sciences – Drug Development Division, Lexington, KY, USA; [2]University of Washington-Seattle, College of Pharmacy, Department of Pharmaceutics, Seattle, WA, USA; [3]GlaxoSmithKline, Analytical Sciences, Product Development, King of Prussia, PA, USA; [4]The Ohio State University College of Medicine, Departments of Pediatrics and Internal Medicine, Nationwide Children's Hospital Lung and Heart-Lung Transplant Programs, Columbus, OH, USA; [5]The Ohio State University, Davis Heart and Lung Research Institute, Columbus, OH, USA; [6]The University of Arizona–Tucson, College of Pharmacy, Skaggs Center of Pharmaceutical Sciences, Tucson, AZ, USA

Correspondence: Heidi M Mansour
The University of Arizona–Tucson, College of Pharmacy, Skaggs Center of Pharmaceutical Sciences, 1703 E Mabel St, Tucson, AZ 85721-0202, USA
Email mansour@pharmacy.arizona.edu

Abstract: The aim of this study was to design and develop respirable antibiotics moxifloxacin (MOXI) hydrochloride and ofloxacin (OFLX) microparticles and nanoparticles, and multifunctional antibiotics particles with or without lung surfactant 1,2-dipalmitoyl-sn-glycero-3-phosphocholine (DPPC) for targeted dry powder inhalation delivery as a pulmonary nanomedicine. Particles were rationally designed and produced by advanced spray-drying particle engineering from an organic solution in closed mode (no water) from dilute solution. Scanning electron microscopy indicated that these particles had both optimal particle morphology and surface morphology, and the particle size distributions were suitable for pulmonary delivery. Comprehensive and systematic physicochemical characterization and in vitro aerosol dispersion performance revealed significant differences between these two fluoroquinolone antibiotics following spray drying as drug aerosols and as cospray-dried antibiotic drug: DPPC aerosols. Fourier transform infrared spectroscopy and confocal Raman microspectroscopy were employed to probe composition and interactions in the solid state. Spray-dried MOXI was rendered noncrystalline (amorphous) following organic solution advanced spray drying. This was in contrast to spray-dried OFLX, which retained partial crystallinity, as did OFLX:DPPC powders at certain compositions. Aerosol dispersion performance was conducted using inertial impaction with a dry powder inhaler device approved for human use. The present study demonstrates that the use of DPPC offers improved aerosol delivery of MOXI as cospray-dried microparticulate/nanoparticulate powders, whereas residual partial crystallinity influenced aerosol dispersion of OFLX and most of the compositions of OFLX:DPPC inhalation powders.

Keywords: lung infection, respiratory, lung surfactant, solid-state particle engineering design, aerosol, fluoroquinolone antibiotic drug delivery

Introduction

Ofloxacin (OFLX) belongs to the fluoroquinolone antimicrobial class, which is widely used due to its excellent antimicrobial activity and good pharmacokinetics properties.[1,2] In tuberculosis treatment, OFLX has been a first-line agent for multidrug-resistant cases, and it has fewer adverse incidences and less severe adverse effects in long-term treatment than the standard agents.[3–5] Moxifloxacin (MOXI) is a fluoroquinolone

broad-spectrum antibacterial agent, shown to be clinically active against Gram-positive microorganisms including *Staphylococcus aureus*, *Streptococcus pneumoniae*, and *Streptococcus pyogenes*. MOXI also has activity against Gram-negative microorganisms including *Haemophilus influenzae*, *Haemophilus parainfluenzae*, *Klebisiella pneumoniae*, *Moraxella catarrhalis*, and against *Mycobacterium tuberculosis*, being as potent as rifampin.[6]

One of the most serious problems with current medicine is the increase in drug resistance among bacterial pathogens, which limits conventional therapy. Research efforts are being made in using a targeted mode of delivery to target the site of infection directly, such as inhalation aerosols for pulmonary infections and by employing nanomedicine.[7–13] Targeted pulmonary delivery of antimicrobials (ie, antibacterials and antifungals) by inhalation aerosols is the subject of much recent interest in research and development, including several clinical trials.[8–11] Pulmonary liposomal aerosol delivery of antimicrobials can effectively fight infections,[14–17] and these liposomal delivery systems can be rendered into inhalable dry powder aerosols.[18] MOXI has been encapsulated in glutaraldehyde-crosslinked chitosan microspheres for intrapulmonary administration.[19] For inhalation applications, OFLX has been encapsulated in glutaraldehyde-crosslinked chitosan microspheres,[20] hyaluronan microspheres for tuberculosis treatment,[21] and as an OFLX–palladium complex encapsulated in biodegradable polymeric microspheres.[22]

The major component of lung surfactant is the phospholipid dipalmitoylphosphatidylcholine (DPPC), which is an essential component in normal lung surfactant, can alleviate compromised lung compliance[23] and is used in nanopharmaceutical applications.[10] Phospholipids are biocompatible, biodegradable excipients that can improve inhaled particle migration to the lung periphery.[24–27] High-dose delivery, higher chemical stability relative to the liquid state, and the potential to tailor particle properties in the solid state are all advantages of dry powder inhalers (DPIs). The aerosol performance of dry powder aerosol formulations is influenced by several particle properties including size distribution, morphology, and particle surface properties, as described in detail.[28–38] Spray-drying is a high-throughput particle engineering design process that offers many advantages in designing and producing tailored particles for DPIs.[28,29] Organic solution advanced spray drying in closed-mode for DPIs has been reported in our previous studies.[39–42]

To the authors' knowledge, this is the first report on the design by organic solution advanced spray drying and comprehensive systematic characterization of inhalable microparticulate/nanoparticulate dry powders of these two fluoroquinolone antibiotics, MOXI and OFLX, for pulmonary delivery as inhalable dry powder aerosols. In addition, organic solution, advanced cospray drying is employed to design microparticulate/nanoparticulate dry powders of MOXI with DPPC and OFLX with DPPC, as lung surfactant mimic multifunctional particles for aerosol delivery, which are comprehensively and systematically characterized for their physicochemical properties and in vitro aerosol performance as respirable dry powders.

Experimental materials and methods

Materials

MOXI hydrochloride United States Pharmacopeia (USP) grade (MOXI, $C_{21}H_{25}ClFN_3O_4$; molecular weight: 437.89 g/mol; ≥99% purity) and OFLX USP grade (OFLX, $C_{18}H_{20}FN_3O_4$; molecular weight: 361.37 g/mol; ≥99% purity) were purchased from APAC Pharmaceutical, LLC (Columbia, MD, USA). Synthetic phospholipid 1,2-dipalmitoyl-*sn*-glycero-3-phosphocholine (DPPC) ($C_{40}H_{80}NO_8P$; molecular weight: 734.04 g/mol) was purchased from Avanti Polar Lipids, Inc., (Alabaster, AL, USA). Their corresponding chemical structures are shown in Figure 1 (ChemDraw® Ultra 10.0, ChemOffice; Cambridgesoft, Waltham, MA, USA). Methanol (high-performance liquid chromatography grade, American Chemical Society-certified grade, purity 99.9%) was obtained from Thermo Fisher Scientific (Pittsburg, PA, USA). HYDRANAL®–Coulomat AD was from Sigma-Aldrich (St Louis, MO, USA). AQUASTAR® anhydrous methanol was from EMD Millipore (Billerica, MA, USA). Water was obtained by Milli-Q POD set-up from EMD Millipore with a resistivity of 18.1 MΩ-cm. All nitrogen gas used for experiments was an ultra-high purity (UHP) nitrogen gas manufactured by Scott-Gross Company, Inc (Lexington, KY, USA). All powders were used as stored in desiccators in the freezer at –23°C. All materials were used as received.

Methods

Preparation of spray-dried particles by organic solution advanced spray-drying (no water) in closed mode

The advanced spray-drying process was performed using the BÜCHI Mini Spray Dryer B-290 coupled with the Inert Loop B-295 and the high-performance cyclone (BÜCHI Labortechnik AG, Flawil, Switzerland). The organic solution spray drying process was in closed mode using UHP dry nitrogen gas as the atomizing gas.

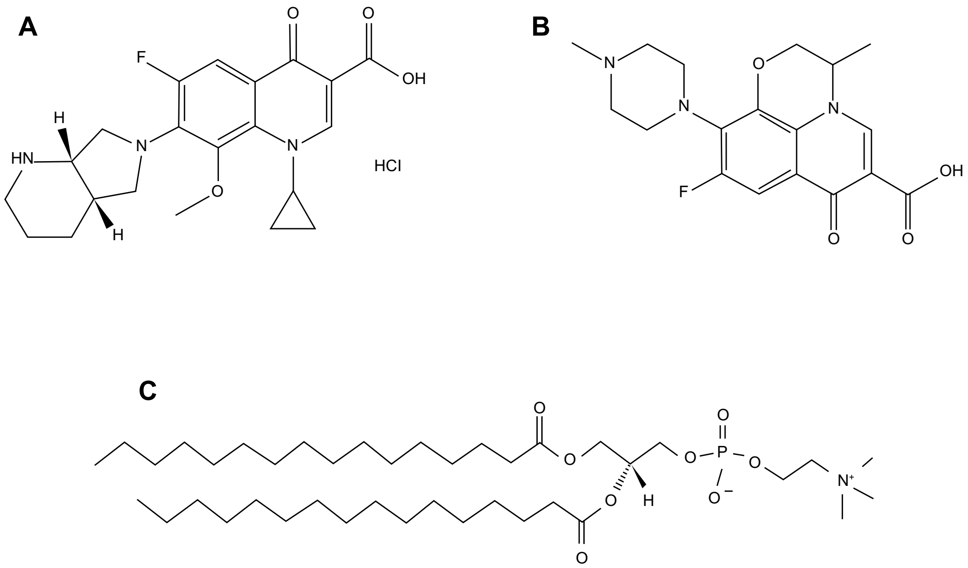

Figure 1 The chemical structures of moxifloxacin hydrochloride, ofloxacin, and dipalmitoylphosphatidylcholine.
Notes: (**A**) Moxifloxacin hydrochloride; (**B**) ofloxacin; (**C**) dipalmitoylphosphatidylcholine.

Spray-dried (SD) and cospray-dried (co-SD) particles at different ratios were obtained by spray drying organic solvent solutions OFLX, MOXI hydrochloride, and/or DPPC under the conditions outlined in Table 1. The feeding solution was prepared by dissolving each component in methanol to make a total concentration of 0.15% w/v. The relative molar ratio of OFLX to DPPC and MOXI to DPPC in the feed solution was100:0, 75:25, 50:50, 25:75, and 0:100, respectively. The feed solution was passed through a stainless steel 0.7 mm diameter atomizing nozzle via a peristaltic feed pump at a flow rate of 15 mL/minute (pump rate 50%). A set inlet temperature of 150°C ± 2°C (primary drying step) resulted in outlet temperatures of 60°C ± 3°C. The atomization gas flow rate was 600 L/hour, and the aspiration rate was 35 m^3/hour (100% aspirator). The resultant dry powder was blown through a high-performance cyclone separator and collected in the sample container. All SD and co-SD powders were stored in glass vials sealed with parafilm in glass desiccators over Drierite™/Indicating Drierite™ (Hammond Drierite Co, Ltd, Xenia, OH, USA) desiccant in the freezer at –23°C under ambient pressure. These are similar conditions as reported previously by our group.[40–43]

Scanning electron microscopy (SEM)

Using conditions previously reported,[39–42] scanning electron microscopy (SEM) of the raw MOXI hydrochloride, raw OFLX, raw DPPC, SD, and co-SD powders were evaluated by SEM, using a Hitachi S-800 microscope (Hitachi Ltd, Tokyo, Japan). Samples were placed on double-sided adhesive carbon tabs (Ted Pella, Inc., Redding, CA, USA),

Table 1 Spray drying conditions for organic solution advanced spray drying in closed-mode under ultra-high purity nitrogen gas for MOXI:DPPC and OFLX:DPPC spray-dried and cospray-dried systems

Formulations	Solvent	Aspiration gas: ultra-high purity nitrogen gas (L/hour)	Inlet temperature (°C)	Outlet temperature (°C)	Pump rate (%)	Aspirator (%)
MOXI:DPPC = 100:0	Methanol	670	150	75	50	100
MOXI:DPPC = 75:25	Methanol	670	150	72	50	100
MOXI:DPPC = 50:50	Methanol	670	150	70	50	100
MOXI:DPPC = 25:75	Methanol	670	150	68	50	100
OFLX:DPPC = 100:0	Methanol	670	150	73	50	100
OFLX:DPPC = 75:25	Methanol	670	150	69	50	100
OFLX:DPPC = 50:50	Methanol	670	150	76	50	100
OFLX:DPPC = 25:75	Methanol	670	150	73	50	100
MOXI/OFLX:DPPC = 0:100	Methanol	670	150	64	50	100

Abbreviations: MOXI, moxifloxacin; DPPC, dipalmitoylphosphatidylcholine; OFLX, ofloxacin.

which were adhered to aluminum stubs (Ted Pella, Inc.), and were coated with gold/palladium alloy thin film using a Hummer VI sputtering system from Technic Inc.. The coating process was operated at 10 AC milliamperes for 3 minutes. The electron beam with an accelerating voltage of 20 kV was used at a working distance of 30 mm. SEM images were captured using Evex NanoAnalysis software (Evex Analytical Instruments, Inc, Princeton, NJ, USA). The average diameters and size distributions were calculated as more than 100 particles using SigmaScan™ Pro 5.0 software (Systat Software Inc., San Jose, CA, USA) for image analysis.

Particle sizing and size distribution

The mean size, standard deviation, and size range of the particles were determined digitally using SigmaScan™ 5.0 software, as previously reported.[41] Using similar conditions as reported,[41] representative micrographs for each particle sample at 5,000× magnification were analyzed by measuring the diameter of at least 100 particles per image with the SigmaScan™ 5.0 software. Data were expressed as number distributions.

X-ray powder diffraction (XRPD)

The crystalline nature (ie, the presence of long-range molecular order) versus non crystallinity (ie, lack of long-range molecular order) of MOXI hydrochloride, OFLX, and DPPC (all as supplied by the manufacturer) SD and co-SD powders, were examined using X-ray powder diffraction (XRPD) (Rigaku Multiflex X-ray diffractometer; Rigaku Corporation, Tokyo, Japan) with a slit-detector Cu Kα radiation (40 kV, 44 mA, and λ = 1.5406 Å) source. The scan range was 5.0°–60.0° (2θ) with a scan rate of 2.00°/minute at ambient temperature. The sample was placed on a horizontal quartz glass sample holder plate. These are similar conditions to those previously reported.[39–42]

Differential scanning calorimetry (DSC)

Using similar conditions previously reported,[39–42] the phase transition of MOXI hydrochloride, OFLX, and DPPC (as supplied by the manufacturer) SD and co-SD formulations were studied by thermogram obtained using the TA Q200 DSC system (TA Instruments, New Castle, DE, USA) equipped with T-Zero® technology and an automated computer-controlled RSC-90 cooling accessory (TA Instruments). Approximately 3 mg of powder was carefully weighed into hermetic anodized aluminum T-Zero® DSC pans (TA Instruments) and sealed with the T-Zero® hermetic sealer (TA Instruments). An empty, hermetically sealed, anodized aluminum pan was used as reference. DSC measurements were performed at the heating rate of 5.00°C/minute from 0°C to 350°C. UHP nitrogen gas (Scott-Gross Company, Inc.,) was used as the purging gas at a purge rate of 50 mL/minute. The glass transition temperature (T_g) was calculated using TA Universal Analysis (TA Instruments).

Attenuated total reflectance infrared (ATR-FTIR) spectroscopy

Fourier transform infrared spectrometry (FTIR) spectra of MOXI hydrochloride, OFLX, and DPPC (as supplied by the manufacturer) SD and co-SD formulations were recorded with a Varian, Inc., 7000e step-scan spectrometer (Agilent Technologies, Santa Clara, CA, USA). An attenuated total reflectance (ATR) accessory was used and the spectra were collected with no further processing of the samples. The powder was placed on the diamond ATR crystal, covered with a glass cover slip, and held in place with a specialized clamp. The spectra were scanned at an 8 cm^{-1} spectral resolution from 700 cm−1 to 4,000 cm^{-1}. The data were collected and analyzed using Varian Resolutions software (Agilent Technologies). These are similar conditions to those previously reported.[41]

Hot-stage microscopy under cross-polarizers

Using similar conditions to those previously reported,[39–42] hot-stage microscopy (HSM) studies were performed under OLYMPUS BX51 polarized microscope (Olympus Corporation, Tokyo, Japan) equipped with an Instec STC200 heating unit and an Instec HCS302 hot stage (Instec, Inc, Boulder, CO, USA). The polarized light was filtered by a γ 530 nm U-TP530 (Olympus Corporation) filter lens. Powder samples were placed on glass slides with cover glass and heated at the rate of 5.00°C/min from 25°C to 350°C. The heating program was controlled by WinTemp software (Instec, Inc). Images were digitally captured by a SPOT Insight digital camera (Diagnostic Instruments, Inc, Sterling Heights, MI, USA).

Confocal Raman microscopy and mapping (chemical imaging)

Using conditions previously reported,[41,44] confocal Raman microscopy[44,45] was performed using a LabRAM confocal dispersive Raman spectrometer and epi-fluorescence microscope system (HORIBA, Ltd, Edison, NJ, USA). The system is equipped with an Olympus BX41 microscope, an Olympus U-LH 100 W Hg lamp, and a U-RFL-T power source used for

fluorescence excitation and brightfield illumination (Olympus America, Inc., Chester Valley, PA, USA). Raman spectra were obtained using a 785 nm diode laser (Sacher Lasertechnik GmbH, Marburg, Germany). The system is also equipped with a 633 nm HeNe laser (CVI Melles Griot, Albuquerque, NM, USA). Raman spectral maps were obtained using a ×20 objective with the stage moved in increments of 10 µm. Each map point was acquired using seven spectral windows, with each window using four accumulations and 2 seconds of detector exposure time. Raman maps required between 18 and 24 hours of total experimental time. A confocal hole of 500 µm and a grating with 600 grooves/mm were used. Spectra were subjected to baseline correction and smoothing prior to further analysis.

In vitro aerosol dispersion performance by Next Generation Impactor™ (NGI)

Aerosolization of the SD and co-SD powders was evaluated using the Next Generation Impactor™ (NGI). In accordance with USP chapter 601 specifications on aerosols,[46] and as previously reported,[39,41] the in vitro aerosol dispersion properties of the dry powder particles as DPIs were determined using the NGI with a stainless steel induction port (ie, USP throat) attachment (NGI model 170; MSP Corporation, Shoreview, MN, USA), equipped with specialized stainless steel NGI gravimetric insert cups (MSP Corporation, Shoreview, MN, USA). Glass fiber filters (55 mm, Type A/E; Pall Life Sciences, Pall Corporation, Exton, Port Washington, NY, USA) were placed in the stainless steel NGI gravimetric insert cups for NGI stages 1 through 7. The NGI was coupled with a Copley TPK 2000 critical flow controller (Copley Scientific, Nottingham, UK), which was connected to a Copley HCP5 vacuum pump (Copley Scientific). The airflow rate, Q, was measured and adjusted prior to each experiment using a Copley DFM 2000 flow meter (Copley Scientific). For Q = 60 L/minute, the D_{a50} aerodynamic cutoff diameters for each NGI stage as calibrated and stated by the manufacturer are 8.06 µm, 4.46 µm, 2.82 µm, 1.66 µm, 0.94 µm, 0.55 µm, and 0.34 µm for stages 1–7, respectively. Three hydroxypropyl methylcellulose hard capsules (size 3; Quali-V®; Qualicaps® Inc, Whitsett, NC, USA) were each loaded with 10 mg of powder per capsule for a total of 30 ± 0.2 mg total per run. The human DPI unit-dose device, the Handihaler® (Boehringer Ingelheim, Germany) was tightly inserted into the induction port via a mouthpiece adapter. The emitted dose (ED), fine particle fraction (FPF), and respirable fraction (RF) were calculated as follows:

$$\text{Emitted dose (ED\%)} = \frac{\text{Initial mass in capsules} - \text{Final mass remaining in capsules}}{\text{Initial mass in capsules}} \times 100\% \quad (1)$$

$$\text{Fine particle fraction (FPF\%)} = \frac{\text{Mass deposited on stages 2 through 7}}{\text{Initial particle mass loaded into capsules}} \times 100\% \quad (2)$$

$$\text{Respirable fraction (RF \%)} = \frac{\text{Mass deposited on stages 2 through 7}}{\text{Initial particle mass on all stages}} \times 100\% \quad (3)$$

The mass median aerodynamic diameter (MMAD) and geometric standard deviation were determined using a mathematic program written by Finlay.[47,48] All experiments were triplicated (n = 3) at ambient temperature and humidity.

Results and discussion

SEM, particle sizing, and size distribution

The surface morphology of MOXI hydrochloride, OFLX, and DPPC (as supplied by the manufacturer), Figure 2, SD and co-SD OFLX:DPPC formulations, as well as the SD and co-SD MOXI:DPPC formulations were investigated by SEM. Figures 3 and 4 show the SEM micrographs, and their corresponding size diameter, standard deviation, and range are tabulated in Table 2, as quantified statistically using SigmaScan™ software.

The SEM micrographs of MOXI hydrochloride (Figure 2A) and DPPC, as supplied by the manufacturer (Figure 2C) show needle-like morphology and a size that is much too large for inhalation. Following organic solution spray drying in closed mode, increasing the DPPC content in the co-SD MOX:DPPC powders changed the particle morphology, as visualized by electron microscopy, from slightly corrugated surface morphology to smooth surface morphology. All particles had spherical particle morphology.

Table 2 Particle size parameters of spray-dried and cospray-dried MOXI:DPPC powders (mean ± standard deviation; n = 3)

Formulations	Diameter (µm)	Range (µm)
MOXI:DPPC = 100:0	0.67 ± 0.19	0.379–1.363
MOXI:DPPC = 75:25	0.70 ± 0.21	0.354–1.406
MOXI:DPPC = 50:50	0.69 ± 0.21	0.403–1.533
MOXI:DPPC = 25:75	0.69 ± 0.22	0.325–1.655
MOXI:DPPC = 0:100	0.64 ± 0.18	0.236–1.166

Abbreviations: MOXI, moxifloxacin; DPPC, dipalmitoylphosphatidylcholine; n, number.

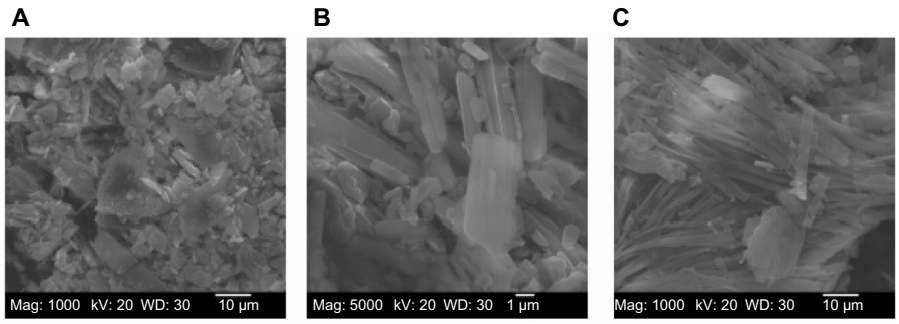

Figure 2 SEM micrographs of (**A**) moxifloxacin hydrochloride (magnification: 1,000×), (**B**) ofloxacin (magnification: 1,000×), and (**C**) DPPC (magnification 1,000×) as supplied by the manufacturer.
Abbreviations: SEM, scanning electron microscope; DPPC, dipalmitoylphosphatidylcholine.

Varying DPPC content from 25% to 75% did not significantly affect the particle size (Table 2). Increasing the concentration of the excipient in the solution to be SD, as well as increasing its methanol content, did not affect particle size.

SD OFLX particles (Figure 4) are spherical in particle morphology. The surface morphology appears to increase in smoothness by increasing the concentration of DPPC from 25% to 75%, but it did not affect particle size (Table 3) significantly. DPPC appears to have a greater effect on the appearance of OFLX particles in terms of surface roughness (surface morphology) than on MOXI particles.

X-ray powder diffraction

XRPD is a direct method for determining the basic information about the structure of a crystalline material.[49] The crystallinity of the pure drug and all SD formulations were examined by studying its XRPD. As shown in Figure 5B, the XRPD diffractogram pattern of OFLX shows distinct sharp diffraction peaks (ie, the presence of long-range molecular order), indicating that the raw drug OFLX, as supplied by the manufacturer, is crystalline. For SD OLFX, co-SD OFLX:DPPC 75:25 and co-SD OFLX:DPPC 50:50 powders still showed these characteristic crystalline OFLX diffraction peaks at 15.77 2θ degree, 19.22 2θ degree, and 26.55 2θ degree, but with reduced peak height (less intense) (ie, residual partial crystallinity exists following spray drying). For co-SD OFLX:DPPC 25:75, there are no sharp diffraction peaks observed, indicating non crystallinity. The diagrams revealed the characteristic peak of the DPPC bilayer multilamellar structure in the solid-state[50] at approximately 21 2θ degrees, which increased in intensity with the addition of DPPC in the SD formulations.

MOXI hydrochloride, as supplied by the manufacturer, was characterized by having an XRPD diffractogram pattern with multiple sharp peaks, which are characteristic of the long-range molecular order present in crystalline materials. Following organic solution spray drying, these characteristic peaks were no longer present, suggesting the loss of crystallinity for all MOXI compositions studied. The characteristic peak of the DPPC at approximately 21 2θ degrees increased with the addition of DPPC in the co-SD MOXI:DPPC formulations. The diagrams revealed the characteristic peak of the DPPC bilayer multilamellar structure in the solid-state[50] at approximately 21 (2θ) degrees.

Differential scanning calorimetry

The thermograms of SD (as supplied by the manufacturer), and different molar ratios of co-SD fluoroquinolone antibiotic

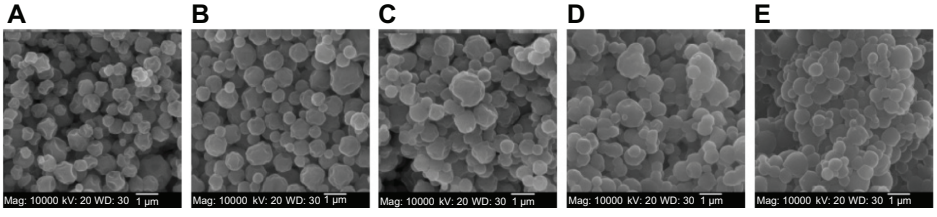

Figure 3 SEM micrographs of SD and co-SD powders.
Notes: (**A**) SD MOXI (magnification: 10,000×); (**B**) co-SD MOXI:DPPC = 75:25 (magnification: 10,000×); (**C**) co-SD MOXI:DPPC = 50:50 (magnification: 10,000×); (**D**) co-SD MOXI:DPPC = 25:75 (magnification 10,000×); and (**E**) SD DPPC (magnification 10,000×).
Abbreviations: SEM, scanning electron microscope; SD, spray-dried; co-SD, cospray-dried; MOXI, moxifloxacin; DPPC, dipalmitoylphosphatidylcholine.

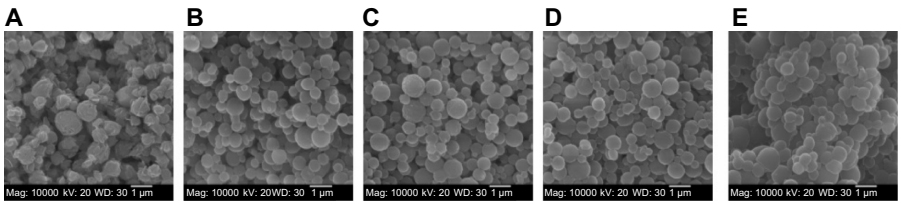

Figure 4 SEM micrographs of SD and co-SD powders.
Notes: (**A**) SD OFLX (magnification: 10,000×); (**B**) co-SD OFLX:DPPC = 75:25 (magnification: 10,000×); (**C**) co-SD OFLX:DPPC = 50:50 (magnification: 10,000×); (**D**) co-SD OFLX:DPPC = 25:75 (magnification 10,000×); and (**E**) SD DPPC (magnification: 10,000×).
Abbreviations: SEM, scanning electron microscope; SD, spray-dried; co-SD, cospray-dried; OFLX, ofloxacin; DPPC, dipalmitoylphosphatidylcholine.

drug:DPPC powders are shown in Figure 6. The OFLX thermogram shows an endothermic peak at 269°C, which represents the melting point of the drug. The thermogram of the co-SD OFLX:DPPC powders shows that the endothermic peak corresponding to the melting point of OFLX is present but reduced. There was no OFLX melting peak when the co-SD OFLX:DPPC molar ratio reached 50:50. The SD OFLX exhibits residual partial crystallinity following organic solution advanced spray drying, as do co-SD OFLX:DPPC at select compositions of 75:25 and 50:50. The presence of residual partial crystallinity agrees well with the XRPD diffractograms.

The thermogram of MOXI shows an endothermic melting peak at 238°C, which is at a lower temperature than that of OFLX. SD MOXI powders show an exothermic peak (ie, a disorder-to-order phase transition) suggestive of crystallization point at 91.7°C. This agrees with the XRPD data, which indicates that the SD MOXI powders are noncrystalline (ie, indicative of amorphous character). With the addition of DPPC to MOXI, the exothermic peak temperatures decreased to 58°C, 52°C, and 50°C for co-SD MOXI:DPPC 75:25, 50:50, and 25:75 powders, respectively. The endothermic peak appeared to also decrease with the addition of DPPC to MOXI, 211°C for SD MOXI versus 136°C for co-SD MOXI:DPPC 75:25 powders.

ATR-FTIR spectroscopy

Infrared spectroscopy is one of most powerful analytical techniques to determine the presence of various functional groups involved in making up the molecule. It provides spectral data regarding any change in the functional group characteristics of a drug molecule occurring while in the processing of a formulation and after spray-drying. FTIR spectra of pure drugs and all formulations are shown in Figure 7.

Table 3 Particle size parameters of spray-dried and cospray-dried OFLX:DPPC powders (mean ± standard deviation; n = 3)

Formulations	Diameter (µm)	Range (µm)
OFLX:DPPC = 100:0	0.69 ± 0.15	0.399–1.293
OFLX:DPPC = 75:25	0.59 ± 0.15	0.326–1.317
OFLX:DPPC = 50:50	0.60 ± 0.18	0.277–1.190
OFLX:DPPC = 25:75	0.57 ± 0.18	0.277–1.178
OFLX:DPPC = 0:100	0.64 ± 0.18	0.236–1.166

Abbreviations: OFLX, ofloxacin; DPPC, dipalmitoylphosphatidylcholine; n, number.

In the FTIR spectra of OFLX, as supplied by the manufacturer, one prominent characteristic peak was found between 3,050 cm^{-1} and 3,000 cm^{-1}, which was assigned to the stretching vibration of the OH group and intramolecular hydrogen bonding (Figure 7). This band also suggested the NH stretching vibration of the imino moiety of piperazinyl groups, which was less prominent due to intense OH stretching vibration. The peak at 2,700 cm^{-1} was assigned to υCH_3 of the methyl group. The band at 1,750–1,700 cm^{-1} represented the acidic carbonyl C = O stretching (ie, $\upsilon C = O$). The peak at 1,650 cm^{-1} to 1,600 cm^{-1} was assigned to the $\upsilon N\text{-}H$ bending vibration of quinolones. The 1,550 cm^{-1} to 1,500 cm^{-1} represented the υCH_2 of the aromatic ring. The band at 1,450–1,400 cm^{-1} was assigned to the stretching vibration of CH_2, confirming the presence of the methylene group in the benzoxazine ring. The peak at 1,400–1,350 cm^{-1} represented the bending vibration of the hydroxyl group. The band at 1,250 cm^{-1} to 1,200 cm^{-1} indicated the stretching vibration of the oxo group. In addition, a strong absorption peak between 1,050 cm^{-1} and 1,000 cm^{-1} was assigned to the C–F group. The band at 900–800 cm^{-1} represented the out of plane bending vibration of double bonded enes or =CH groups. These characteristic peaks also appeared in the formulations of single OFLX, co-SD OF-DPPC 75:25, and co-SD OF-DPPC 50:50 powders, while peak strengths were getting weaker with increasing content of DPPC. MOXI hydrochloride was characterized by having an infrared spectrum with peaks at approximately 3,359 cm^{-1}, 2,974 cm^{-1}, 1,716 cm^{-1}, 1,467 cm^{-1}, 1,137 cm^{-1}, and 952 cm^{-1} in the pure drug. The presence of the same peaks, which are characteristic functional groups of the drug and DPPC, observed in the drug polymer physical mixture confirm that there is no incompatibility between the drug and DPPC.

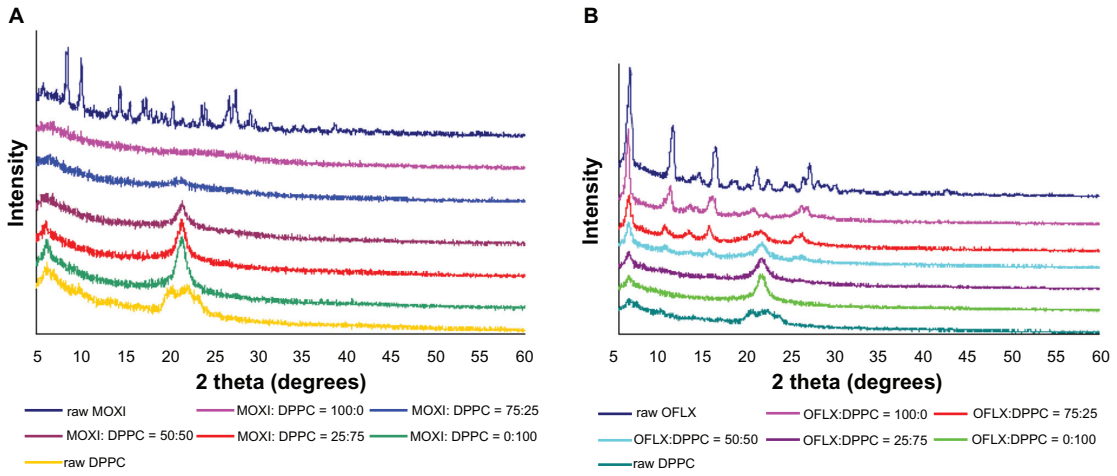

Figure 5 XRPD diffractograms of MOXI hydrochloride, OFLX, and DPPC (supplied by the manufacturer) spray-dried and cospray-dried powders at various molar ratios.
Notes: (**A**) MOXI:DPPC; (**B**) OFLX:DPPC.
Abbreviations: MOXI, moxifloxacin; DPPC, dipalmitoylphosphatidylcholine; OFLX, ofloxacin; XRPD, X-ray powder diffraction.

HSM under cross-polarizers

The MOXI hydrochloride, OFLX and DPPC as supplied by the manufacturer, and their SD and co-SD powders were visualized by HSM for the presence/absence of birefringence and visual changes with increasing temperature. Representative images are shown in Figures 8–11. All samples appeared unchanged at 37°C (physiological temperature).

While for MOXI hydrochloride, as supplied by the manufacturer (Figure 9), and OFLX, as supplied by the manufacturer (Figure 10), the birefringence and the crystal shape of drug as supplied by the manufacturer were observed over nearly the entire temperature range studied under cross-polarized light. The melting process occurred at ~270°C for OFLX and ~235°C for MOXI, as evident by liquid droplet formation clearly seen in the micrographs, which was in good agreement with the DSC thermal analysis data. No birefringence was observed in SD OFLX samples (Figure 10) before it melted, but the birefringence appeared

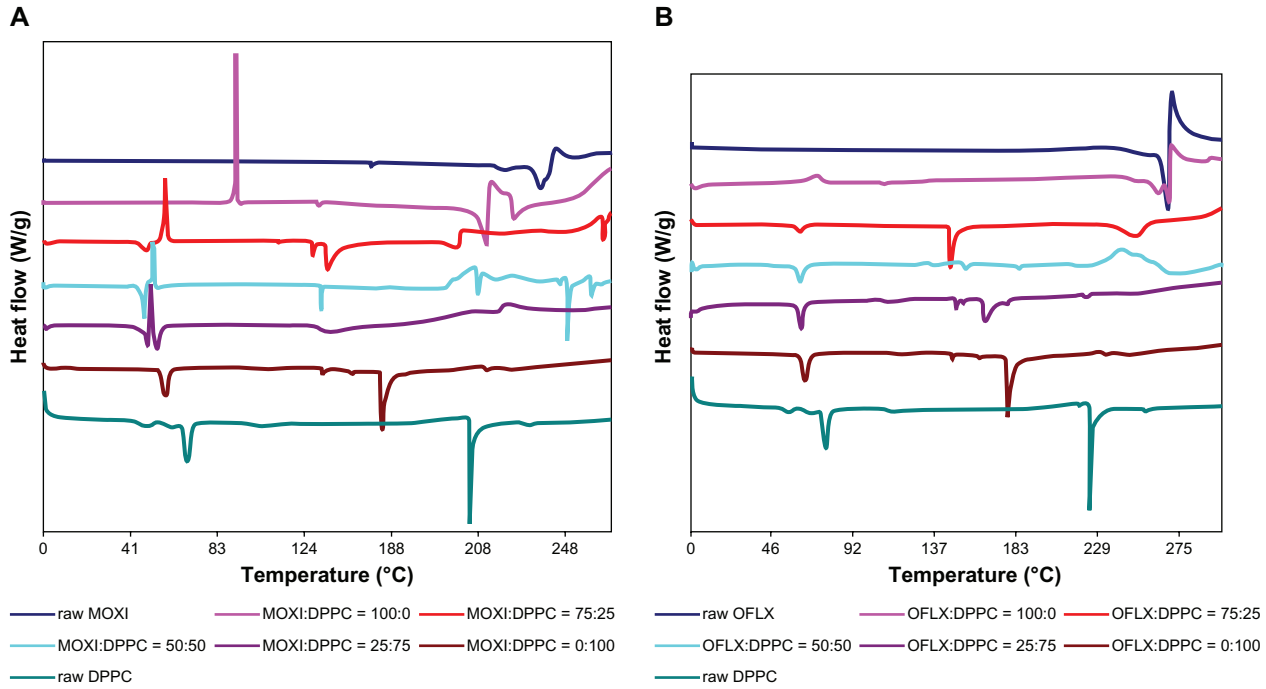

Figure 6 DSC thermograms of MOXI hydrochloride, OFLX, and DPPC (supplied by the manufacturer) spray-dried and cospray-dried powders at various molar ratios.
Notes: (**A**) MOXI:DPPC; (**B**) OFLX:DPPC.
Abbreviations: MOXI, moxifloxacin; DPPC, dipalmitoylphosphatidylcholine; OFLX, ofloxacin; DSC, differential scanning calorimetry.

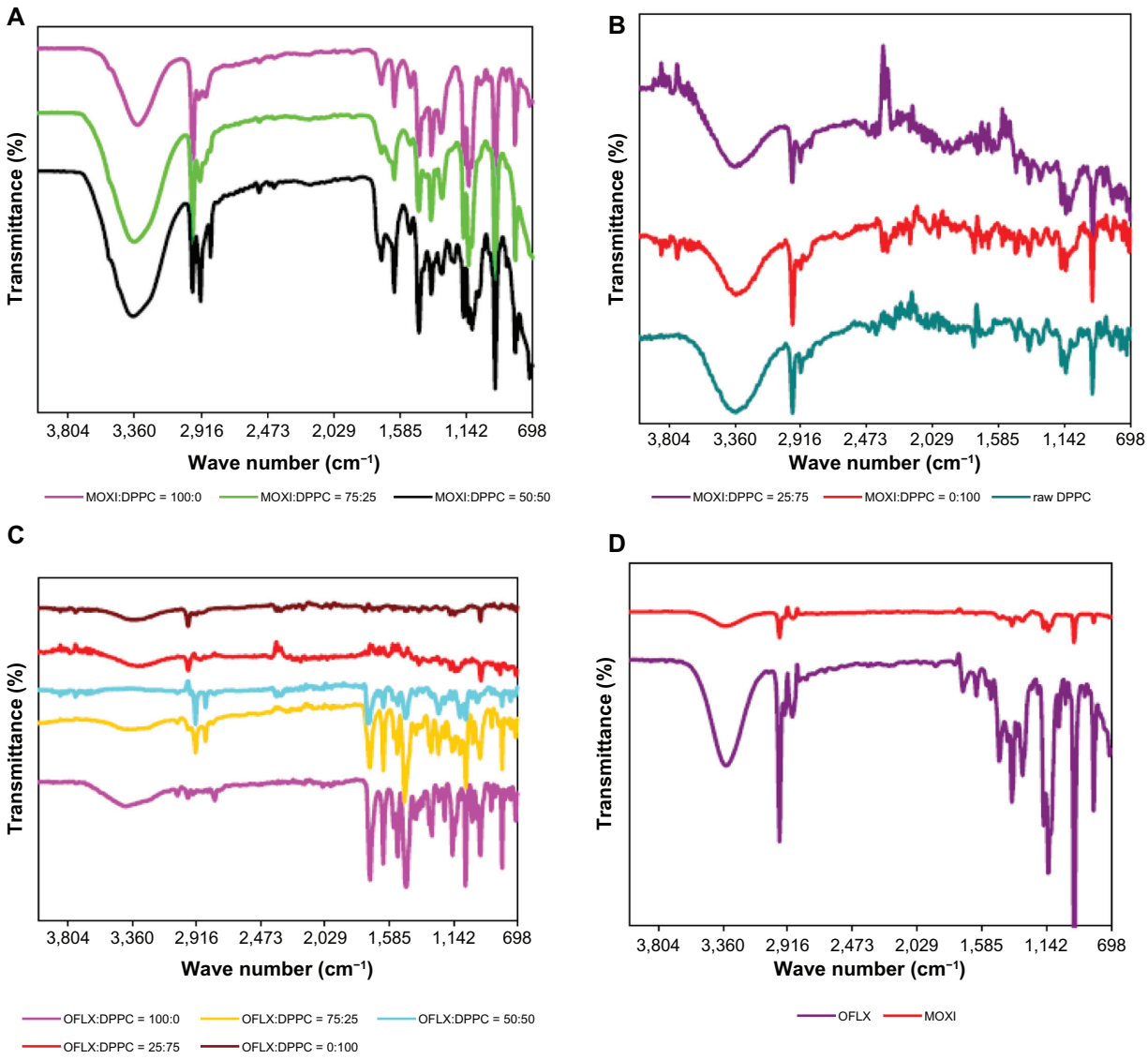

Figure 7 ATR-FTIR spectra of MOXI hydrochloride, OFLX, and DPPC (supplied by the manufacturer) spray-dried and cospray-dried powders at various molar ratios.
Notes: (**A** and **B**) MOXI:DPPC; (**C**) OFLX:DPPC; and (**D**) MOXI hydrochloride and OFLX supplied by the manufacturer.
Abbreviations: MOXI, moxifloxacin; DPPC, dipalmitoylphosphatidylcholine; OFLX, ofloxacin; ATR-FTIR, attenuated total reflectance infrared–Fourier transform infrared spectroscopy.

after melting. For SD MOXI, it showed dark agglomerates lacking birefringence over the whole temperature range under cross-polarized light, which indicated a noncrystalline amorphous character, which was in good agreement with the XRPD and DSC data. Birefringence was seen in DPPC, as supplied by the manufacturer samples, as well as in SD DPPC powders before and after it melted (Figure 8), which was in good agreement with its liquid crystalline self-assembly phase behavior.

Co-SD MOXI:DPPC 75:25 powders showed dark agglomerates lacking birefringence across the whole temperature range, as would be expected for noncrystalline amorphous materials. For co-SD OFLX:DPPC 75:25 formulations, after dynamic heating to 100°C, the birefringence started to diminish. This phase transition may correspond to the melting of DPPC. Melting was visualized at temperatures of 260°C for co-SD OFLX-DPPC 75:25, as evident by liquid droplet formation seen in the micrographs. Although the thermal behavior is complex, these results are in good agreement with the DSC thermograms (Figure 6).

Confocal Raman microscopy and mapping (chemical imaging)

Confocal Raman microscopy analysis was performed using a 785 nm laser, since 633 nm laser irradiation was found to cause strong fluorescence emissions that overwhelmed the

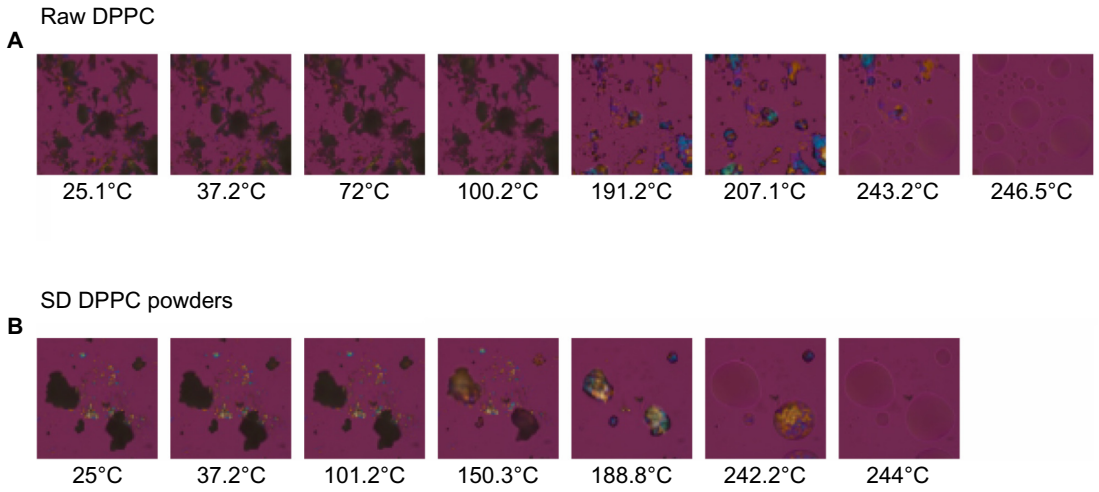

Figure 8 Representative HSM micrographs for DPPC supplied by the manufacturer versus SD DPPC powders.
Notes: (**A**) Raw DPPC; (**B**) SD DPPC powders.
Abbreviations: DPPC, dipalmitoylphosphatidylcholine; SD, spray-dried; HSM, hot-stage microscopy.

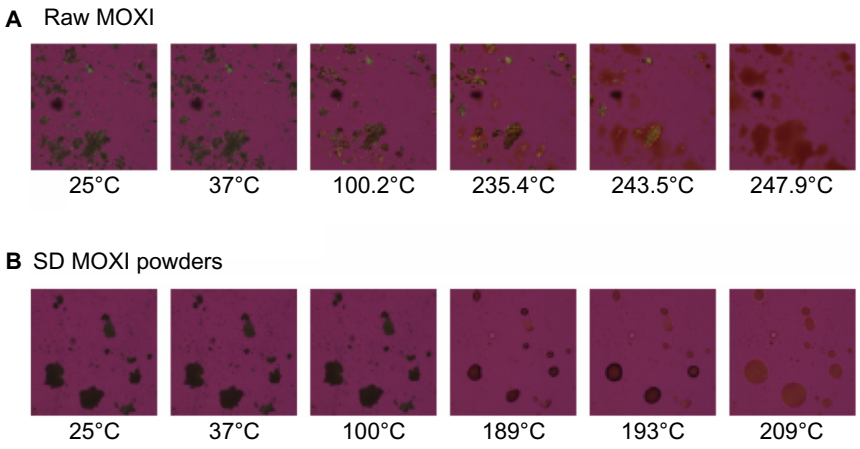

Figure 9 Representative HSM micrographs for MOXI hydrochloride supplied by the manufacturer versus SD MOXI powders.
Notes: (**A**) Raw MOXI; (**B**) SD MOXI.
Abbreviations: MOXI, moxifloxacin; SD, spray-dried; HSM, hot-stage microscopy.

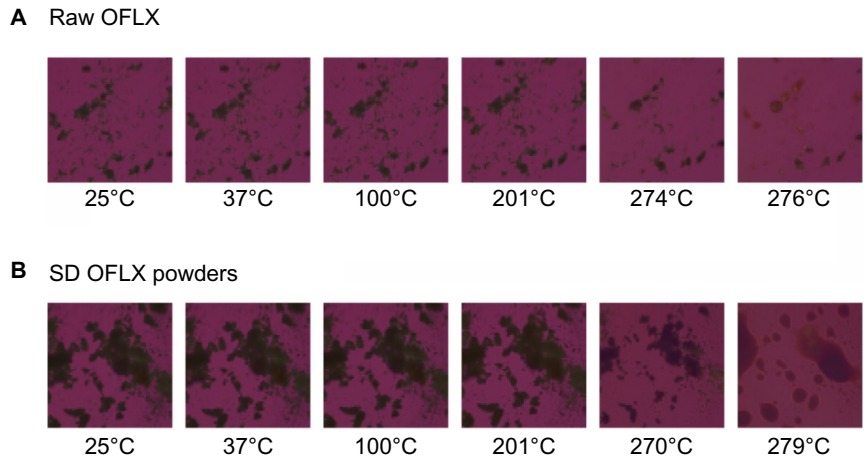

Figure 10 Representative HSM micrographs for OFLX supplied by the manufacturer versus SD OFLX powders.
Notes: (**A**) Raw OFLX; (**B**) SD OFLX.
Abbreviations: OFLX, ofloxacin; SD, spray-dried; HSM, hot-stage microscopy.

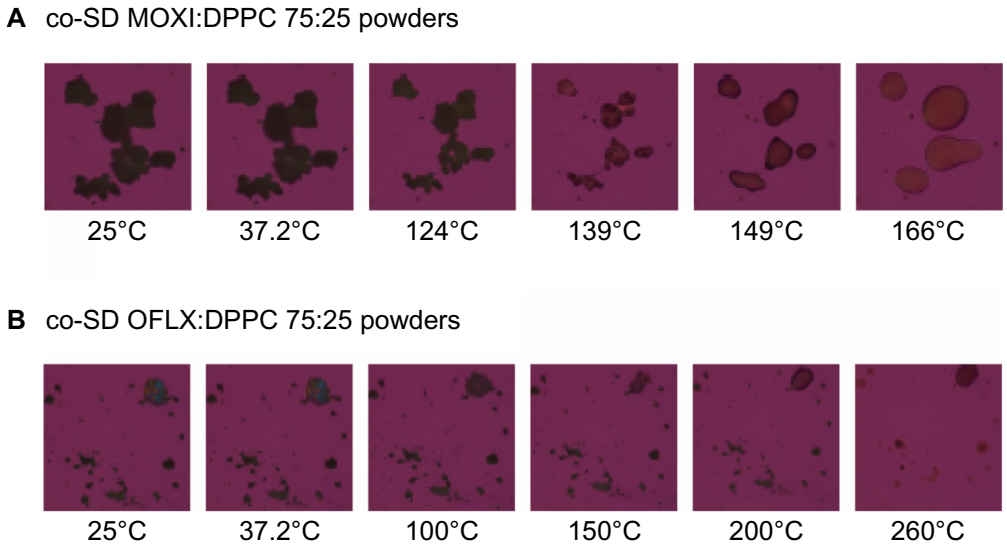

Figure 11 Representative HSM micrographs for co-SD MOXI:DPPC 75:25 versus co-SD OFLX:DPPC 75:25 powders.
Abbreviations: co-SD, cospray-dried; MOXI, moxifloxacin; DPPC, dipalmitoylphosphatidylcholine; HSM, hot-stage microscopy; OFLX, ofloxacin.

Raman spectra. Raman spectra of MOXI hydrochloride, OFLX, and DPPC, as supplied by the manufacturer, are compared to the spectra of SD OFLX and SD MOXI in Figure 12. Both MOXI and OFLX as supplied by the manufacturer, and SD MOXI and OFLX showed only minimal Raman intensity in the region around 3,000 cm^{-1}. DPPC showed strong Raman scattering in the 2,950 to 2,830 cm^{-1} range arising from aliphatic chains and between 1,105 cm^{-1} and 1,085 cm^{-1}. Both of these bands are specific for DPPC in the presence of either antibiotic compound and allow for Raman mapping

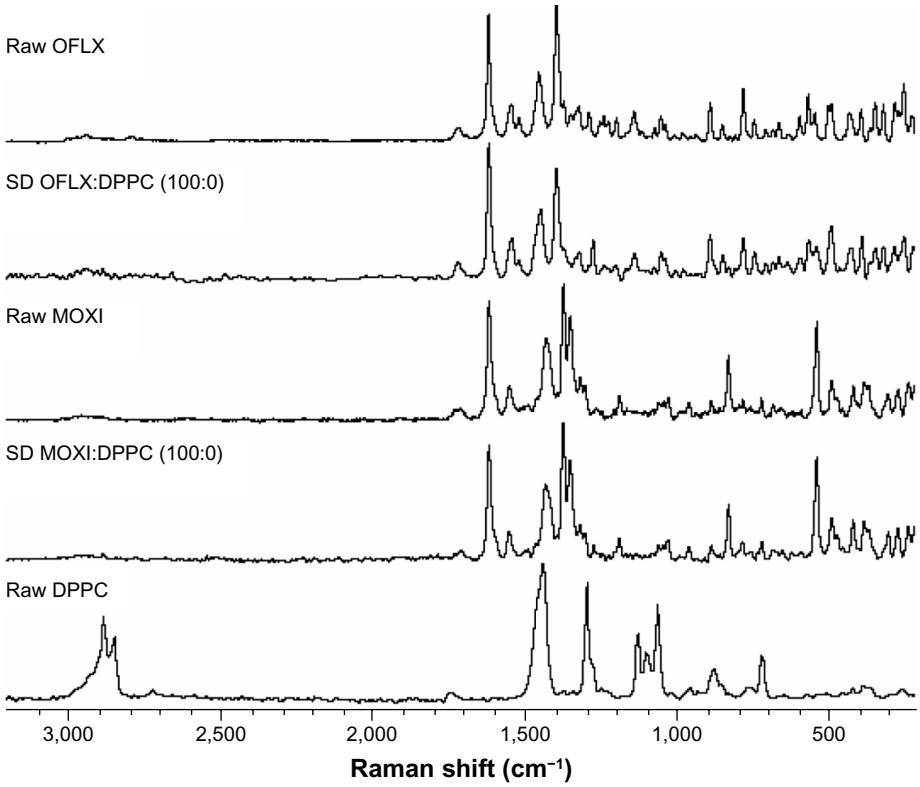

Figure 12 Raman spectra obtained via confocal microscopy of OFLX, MOXI, and DPPC (supplied by the manufacturer) shown in comparison to representative spectra obtained from SD MOXI:DPPC (100:0) and OFLX:DPPC (100:0) particles.
Abbreviations: OFLX, ofloxacin; SD, spray-dried; DPPC, dipalmitoylphosphatidylcholine; MOXI, moxifloxacin.

of the composition and distribution of drug and DPPC in SD particles. The Raman spectra of SD MOXI and OFLX were indistinguishable from their raw crystalline counterparts. In the case of OFLX, this result is consistent with the XRPD results presented previously that indicated no change in crystalline form upon spray drying for OFLX without DPPC. In the case of MOXI, where amorphous material was observed in the bulk sample obtained from spray drying without DPPC, the Raman spectrum indicates that crystallization has occurred in the surface region sampled by confocal microscopy, most likely during storage.

A Raman map of an agglomerated particle of co-SD MOXI:DPPC 50:50 is shown in Figure 13A. A band ratio analysis was performed using the band area of the region of 1,640 cm^{-1} to 1,585 cm^{-1}, which is characteristic of MOXI, and the aforementioned band area in the region of 1,105 cm^{-1} to 1,085 cm^{-1} that is specific for DPPC. The results of this analysis are superimposed on the brightfield optical image in Figure 13A, where the brighter blue–green color is indicative of greater MOXI content relative to DPPC. The overall band ratio variance is minor. This indicates that the particle composition is generally homogeneous. Spectra extracted from three points on the map, as shown in Figure 13B, confirm this finding. No indication of inhomogeneity with respect to form was observed. The Raman results shown in Figure 13 were representative of the results observed for other agglomerated SD particles with different drug-to-lipid ratios.

Using the same band areas, a Raman map of an agglomerated particle of co-SD OFLX:DPPC 50:50 was plotted as shown in Figure 14A. Because of their structural similarity, a strong band that is characteristic of OFLX occurs in the same region as for MOXI, as seen in Figure 12. The band ratio map of co-SD OFLX:DPPC 50:50 showed minor indications of inhomogeneity. Spectra extracted from three points in this map are shown in Figure 14B, and minor variations in the peaks assigned to OFLX are seen relative to those assigned to DPPC; however, the overall drug distribution in the particles was still homogeneous.

Fluorescence microscopy of MOXI and OFLX, as supplied by the manufacturer, showed strong fluorescence emission from these compounds, in agreement with the results from the Raman experiments using 633 nm laser irradiation. No detectable fluorescence was obtained from DPPC as supplied by the manufacturer. Fluorescence microscopy was used to image particles to assess the homogeneity of drug distribution, which was also found to be homogeneous, in agreement

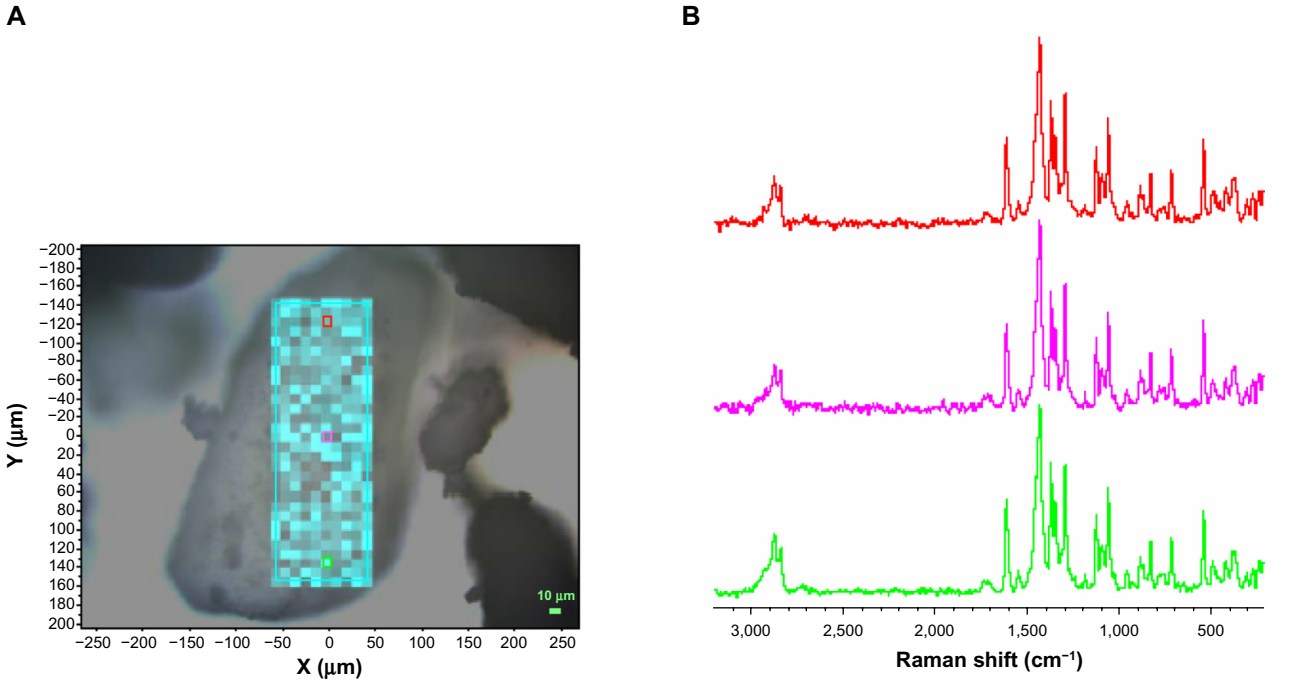

Figure 13 Raman band area ratio map of the MOXI to DPPC ratio in agglomerated spray-dried particles and extracted spectra from three points that illustrate the homogeneous distribution of MOXI and DPPC across the mapped region.
Notes: (**A**) Raman band area ratio map of the MOXI to DPPC ratio in agglomerated spray-dried particles (MOXI:DPPC 50:50) superimposed on a brightfield optical image. Increasing blue–green color is associated with greater concentration of MOXI relative to DPPC. The map sampled a 10 × 30 rectangle using 10 µm stage increments, and a full spectrum was acquired at each point. (**B**) Extracted spectra from three points (denoted by red, purple, and green-bordered rectangles in [**A**]) that illustrate the homogeneous distribution of MOXI and DPPC across the mapped region.
Abbreviations: MOXI, moxifloxacin; DPPC, dipalmitoylphosphatidylcholine.

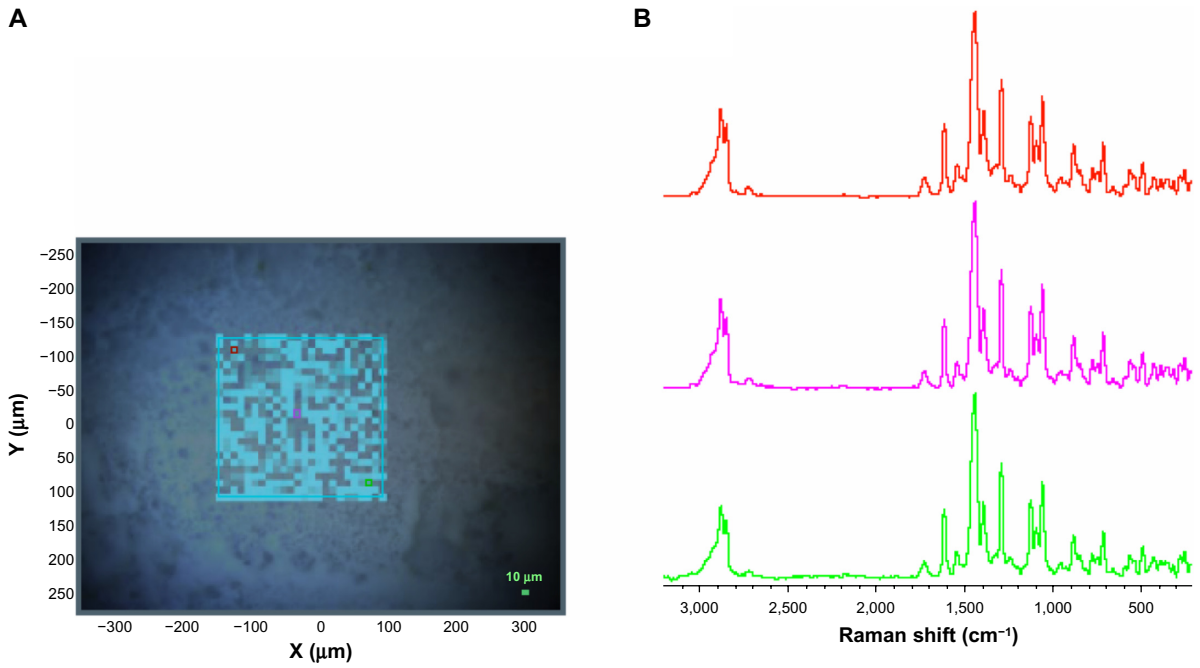

Figure 14 Raman band area ratio map of the OFLX to DPPC ratio in agglomerated spray-dried particles and extracted spectra from three points that illustrate the homogeneous distribution of OFLX and DPPC across the mapped region.
Notes: (**A**) Raman band area ratio map of the OFLX to DPPC ratio in agglomerated spray-dried particles (OFLX:DPPC 50:50) superimposed on a brightfield optical image. Increasing blue–green color is associated with greater concentration of OFLX relative to DPPC. The map sampled a 24 × 24 region using 10 µm stage increments, and a full spectrum was acquired at each point. (**B**) Extracted spectra from three points (denoted by red, purple, and green-bordered rectangles in [**A**]) that illustrate the homogeneous distribution of OFLX and DPPC across the mapped region.
Abbreviations: OFLX, ofloxacin; DPPC, dipalmitoylphosphatidylcholine.

with the Raman microscopy results. Two representative images are shown in Figure 15 for the materials prepared with the lowest concentration of antibiotic, co-SD MOXI:DPPC 25:75 and co-SD OFLX:DPPC 25:75, where the sensitivity of fluorescence microscopy is most advantageous. The images shown in Figure 15 can be obtained in real time at video rates in comparison to the extended times (22 hours) required for the lower-resolution Raman maps shown here with 785 nm laser irradiation.

In vitro aerosol dispersion performance by NGI

The aerosol deposition plots for all SD and co-SD powders using NGI are shown in Figure 16 (dispersion plots), and the

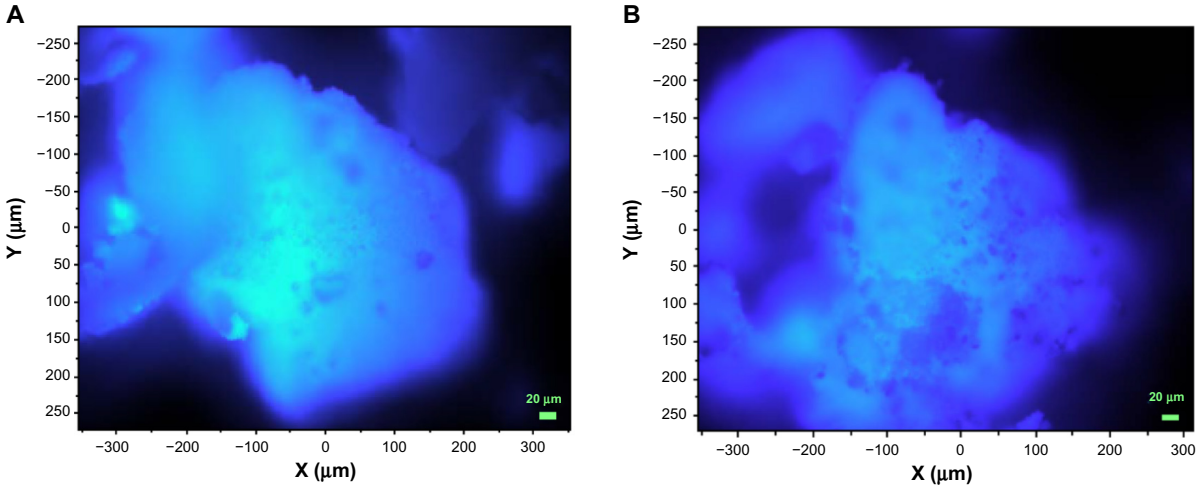

Figure 15 Fluorescence microscopy images showing the overall homogeneity of drug distribution in agglomerated particles.
Notes: (**A**) MOXI:DPPC (25:75); (**B**) OFLX:DPPC (25:75). Images were obtained using a 20× objective.
Abbreviations: MOXI, moxifloxacin; DPPC, dipalmitoylphosphatidylcholine; OFLX, ofloxacin.

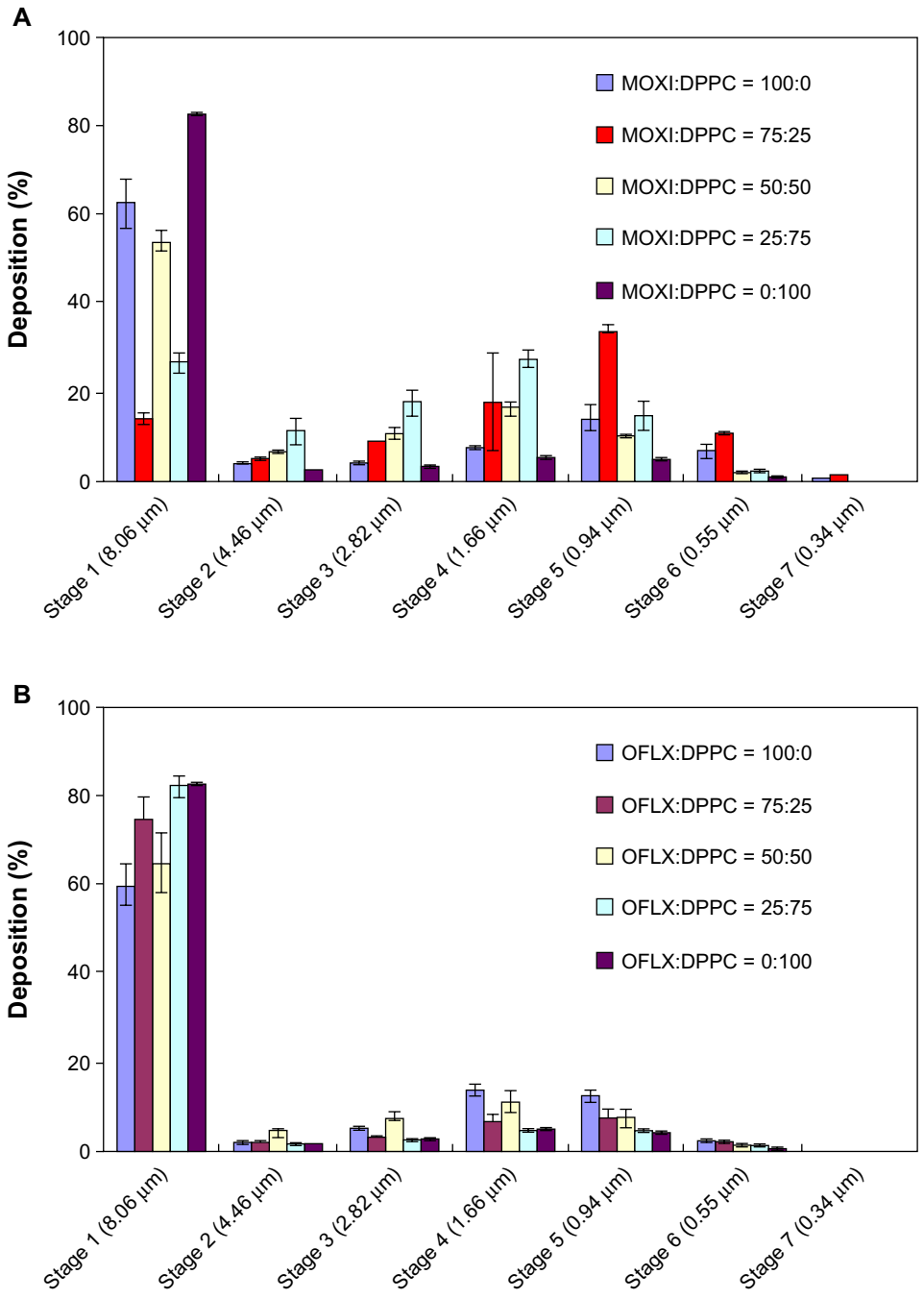

Figure 16 In vitro aerosol dispersion performance as the percent of deposition at each stage of the Next Generation Impactor™ at Q = 60 L/minute with the Handihaler® DPI device for dry powder inhalation aerosols.
Notes: (**A**) SD and co-SD MOXI:DPPC; (**B**) SD and co-SD OFLX:DPPC.
Abbreviations: MOXI, moxifloxacin; DPPC, dipalmitoylphosphatidylcholine; OFLX, ofloxacin; Q, airflow rate; DPI, dry powder inhaler; SD, spray-dried; co-SD, cospray-dried.

aerosol dispersion parameters are tabulated in Tables 4 and 5. Measurable stage deposition on all seven NGI stages for all SD and co-SD powders was observed. Aerosol dispersion performance values of ED, FPF, and RF are high for all SD and co-SD powders. The stage deposition percentage varied with respect to DPPC content and also the drug effect of MOXI versus OFLX in the co-SD powders is evident when comparing Figure 16A versus Figure 16B.

The presence of DPPC with MOXI influenced the co-SD MOXI:DPPC aerosol deposition behavior (Figure 16A). The powders exhibited excellent aerosolization properties with ED values greater than 90% for most compositions and

Table 4 Aerosol dispersion performance parameters as aerosolized dry powders of SD and co-SD for MOXI:DPPC including ED, FPF, RF, MMAD, and GSD

SD and co-SD powders	ED (%)	FPF (%)	RF (%)	MMAD (μm)	GSD
MOXI:DPPC = 100:0	92.85 ± 1.76	57.17 ± 1.94	37.48 ± 5.55	5.61 ± 2.15	3.42 ± 0.57
MOXI:DPPC = 75:25	86.35 ± 2.11	66.66 ± 0.79	85.68 ± 1.24	1.76 ± 0.04	1.76 ± 0.02
MOXI:DPPC = 50:50	96.71 ± 0.56	56.64 ± 0.72	46.04 ± 2.11	5.24 ± 0.23	2.61 ± 0.16
MOXI:DPPC = 25:75	94.08 ± 2.88	48.08 ± 2.97	73.36 ± 2.07	3.13 ± 0.35	1.93 ± 0.06
MOXI:DPPC = 0:100	95.85 ± 1.78	57.45 ± 1.26	17.62 ± 0.75	22.55 ± 1.15	4.83 ± 0.08

Notes: Mean ± standard deviation; n = 3.
Abbreviations: SD, spray-dried; co-SD, cospray-dried; MOXI, moxifloxacin; DPPC, dipalmitoylphosphatidylcholine; ED, emitted dose; FPF, fine particle fraction; RF, respirable fraction; MMAD, mass median aerodynamic diameter; GSD, geometric standard deviation; n, number.

FPF values up to 67% (Table 4). All of the MMAD values for SD MOXI and co-SD MOXI:DPPC aerosols (Table 4) were suitable for effectively reaching the smaller airways. Co-SD MOXI:DPPC 75:25, 50:50, and 25:75 exhibited high RF values of 85.68% ± 1.24%, 46.04% ± 2.11%, and 73.36% ± 2.07%, respectively. Co-SD MOXI:DPPC 75:25 showed the highest deposition on stage 5. A shift in the deposition pattern of co-SD MOXI:DPPC towards the lower NGI stages (Stages 4–5) is also observed.

The NGI stage deposition plots (Figure 16B) show that agglomerated particles deposit on stage 1 for the SD OFLX and co-SD OFLX powders followed by significant deposition on the remaining stages, particularly during stages 4–6. SD OFLX and co-SD OFLX:DPPC 75:25 and 50:50 compositions gave significantly higher deposition on the stages with D_{a50} aerodynamic cutoff nanometer values than the co-SD OFLX 25:75 and SD DPPC powders. As indicated from DSC thermal analysis and XRPD diffraction patterns, SD and co-SD OFLX:DPPC 75:25 and 50:50 exhibited partial residual crystallinity, and this appears to influence aerosol dispersion performance of the OFLX fluoroquinolone antibiotic system. The presence of residual partial crystallinity appears to influence the degree of observed surface roughness from a corrugated surface morphology to smooth surface morphology and spherical particle morphology (Figure 4), with increasing DPPC content. A comparison of SD DPPC versus SD OFLX aerosols indicated that SD OFLX had a statistically significant higher RF value of 39.75% ± 4.38% when compared to the SD DPPC RF value of 17.62% ± 0.75%. Analysis of the deposition profiles of the co-SD OFLX aerosols containing different molar ratios DPPC exhibited significantly different deposition profiles when compared to SD OFLX.

The MMAD values for the co-SD 25:75 ratio for both OFLX:DPPC and MOXI:DPPC aerosols were larger than for the co-SD 75:25 ratio, although SEM image analysis showed a similar primary particle size for them. This suggests that DPPC has a significant hydrophobic effect on the aerodynamic behavior for these ratios. The morphology evaluation (Figures 3 and 4) showed that the MOXI:DPPC and OFLX:DPPC particles in the dried formulations were rendered smaller and more spherical than the MOXI and OFLX particles supplied by the manufacturer (Figure 2). Solid surface morphological modifications, due to the presence of surface-active lung surfactant-mimic DPPC, may influence the dry powder aerosol dispersion of these two antibiotics particles by favorably decreasing interparticle interactions. The morphology of SD particles is affected by the rate of solvent evaporation during the spray-drying process, and the wrinkled particles may result from the build-up of vapor pressure within the particle leading to its collapse. In our novel advanced organic solution spray-drying method,

Table 5 Aerosol dispersion performance parameters as aerosolized dry powders of SD and co-SD for OFLX:DPPC including ED, FPF, RF, MMAD, and GSD

SD and co-SD powders	ED (%)	FPF (%)	RF (%)	MMAD (μm)	GSD
OFLX:DPPC = 100:0	90.51 ± 8.43	62.59 ± 3.70	39.75 ± 4.38	5.30 ± 1.03	2.85 ± 0.19
OFLX:DPPC = 75:25	96.96 ± 0.76	67.77 ± 0.92	25.25 ± 5.02	13.23 ± 4.97	4.42 ± 0.60
OFLX:DPPC = 50:50	96.52 ± 2.33	59.52 ± 3.89	34.92 ± 6.53	8.52 ± 2.64	3.22 ± 0.35
OFLX:DPPC = 25:75	97.40 ± 0.82	63.35 ± 0.81	17.80 ± 2.44	23.27 ± 5.32	5.14 ± 2.67
OFLX:DPPC = 0:100	95.85 ± 1.78	57.45 ± 1.26	17.62 ± 0.75	22.55 ± 1.58	4.83 ± 0.08

Notes: Mean ± standard deviation; n = 3.
Abbreviations: SD, spray-dried; co-SD, cospray-dried; OFLX, ofloxacin; DPPC, dipalmitoylphosphatidylcholine; ED, emitted dose; FPF, fine particle fraction; RF, respirable fraction; MMAD, mass median aerodynamic diameter; GSD, geometric standard deviation; n, number.

methanol was used to solubilize the drug and DPPC together as a dilute solution, which reduces the final particle size in the solid state. This method also reduces the residual water content in the final respirable powders which, in turn, enhances aerosol dispersion performance by reducing capillary forces that act between the surfaces of adjacent particles.

Conclusion

Dry powder inhalational delivery of antibiotics has great potential in the effective treatment of pulmonary infections in a targeted manner, while reducing the growing complication of bacterial drug resistance. The design, comprehensive characterization, and in vitro aerosol dispersion performance of microparticulate/nanoparticulate MOXI and OFLX inhalation aerosol antibiotic powders by organic solution-advanced spray-drying in closed mode from methanol solution (no water) was achieved. In addition, lung surfactant-mimic multifunctional particles in the solid state were produced as inhalable dry powders for each fluoroquinolone antibiotic at several molar ratios. The small particle size, unimodal narrow size distribution, spherical particle morphology, and smooth surface morphology were all suitable for targeted respiratory drug delivery as DPIs. There were also changes in the physical properties after processing where the OFLX powders retained partial crystallinity for SD OFLX and co-SD OFLX:DPPC at molar ratios of 75:25 and 50:50, whereas the SD MOXI and co-SD MOXI:DPPC powders were rendered noncrystalline (amorphous) at all compositions studied. The present study demonstrates that the use of DPPC with MOXI enhances aerosol performance as respirable co-SD powders versus SD MOXI. It was interesting to find that DPPC can influence particle shape and surface morphology of OFLX in the solid state by affecting residual partial crystallinity.

Acknowledgments

The authors thank Dr Dicky Sick Ki Yu for SEM access, Dr Tonglei Li for XRPD and HSM access, and Dr Hilt for ATR-FTIR access at the University of Kentucky. The authors gratefully acknowledge Visiting Scholarship support to Dr Jinghua Duan. The authors gratefully acknowledge fellowship support from the UK Center of Membrane Sciences, the Graduate School Academic Year Fellowship, and the Daniel R Reedy Quality Achievement Fellowship awarded to Xiaojian Li.

Disclosure

The authors report no conflicts of interest in this work.

References

1. Todd PA, Faulds D. Ofloxacin. A reappraisal of its antimicrobial activity, pharmacology and therapeutic use. *Drugs*. 1991;42(5):825–876.
2. Ludwig E. Controversies on pharmacokinetics of fluoroquinolones in elderly patients. *Int J Antimicrob Agents*. 1993;3(1):49–59.
3. Humma LM. Prevention and treatment of drug-resistant tuberculosis. *Am J Health Syst Pharm*. 1996;53(19):2291–2298; quiz 2335.
4. Alangaden GJ, Lerner SA. The clinical use of fluoroquinolones for the treatment of mycobacterial diseases. *Clin Infect Dis*. 1997;25(5):1213–1221.
5. Kawahara S, Tada A, Nagare H. Clinical evaluation of new quinolones as antituberculosis drugs. *Kekkaku*. 1999;74(1):71–75. Japanese.
6. Gosling RD, Uiso LO, Sam NE, et al. The bactericidal activity of moxifloxacin in patients with pulmonary tuberculosis. *Am J Respir Crit Care Med*. 2003;168(11):1342–1345.
7. Mansour HM, Rhee YS, Wu X. Nanomedicine in pulmonary delivery. *Int J Nanomedicine*. 2009;4:299–319.
8. Song JH. What's new on the antimicrobial horizon? *Int J Antimicrob Agents*. 2008;32 Suppl 4:S207–S213.
9. Garcia-Contreras L, Hickey AJ. Pharmaceutical and biotechnological aerosols for cystic fibrosis therapy. *Adv Drug Deliv Rev*. 2002;54(11):1491–1504.
10. Mansour HM, Rhee YS, Park CW, DeLuca PP. Lipid nanoparticulate drug delivery and nanomedicine. In: Moghis A, editor. *Lipids in Nanotechnology*. 1st ed. Urbana, IL: American Oil Chemists Society (AOCS) Press; 2011:221–268.
11. Hayes D Jr, Murphy BS, Mullett TW, Feola DJ. Aerosolized vancomycin for the treatment of MRSA after lung transplantation. *Respirology*. 2010;15(1):184–186.
12. Pison U, Welte T, Giersig M, Groneberg DA. Nanomedicine for respiratory diseases. *Eur J Pharmacol*. 2006;533(1–3):341–350.
13. Kurmi BD, Kayat J, Gajbhiye V, Tekade RK, Jain NK. Micro- and nanocarrier-mediated lung targeting. *Expert Opin Drug Deliv*. 2010;7(7):781–794.
14. Park CW, Hayes D Jr, Mansour HM. Pulmonary inhalation aerosols for targeted antibiotics drug delivery. *European Pharmaceutical Review*. 2011;16(1):32–36.
15. Gilbert BE. Liposomal aerosols in the management of pulmonary infections. *J Aerosol Med*. 1996;9(1):111–122.
16. Okusanya OO, Bhavnani SM, Hammel J, et al. Pharmacokinetic and pharmacodynamic evaluation of liposomal amikacin for inhalation in cystic fibrosis patients with chronic pseudomonal infection. *Antimicrob Agents Chemother*. 2009;53(9):3847–3854.
17. Weers J, Metzheiser B, Taylor G, Warren S, Meers P, Perkins WR. A gamma scintigraphy study to investigate lung deposition and clearance of inhaled amikacin-loaded liposomes in healthy male volunteers. *J Aerosol Med Pulm Drug Deliv*. 2009;22(2):131–138.
18. Willis L, Hayes D Jr, Mansour HM. Therapeutic liposomal dry powder inhalation aerosols for targeted lung delivery. *Lung*. 2012;190(3):251–262.
19. Ventura CA, Tommasini S, Crupi E, et al. Chitosan microspheres for intrapulmonary administration of moxifloxacin: interaction with biomembrane models and in vitro permeation studies. *Eur J Pharm Biopharm*. 2008;68(2):235–244.
20. Park JH, Jin HE, Kim DD, Chung SJ, Shim WS, Shim CK. Chitosan microspheres as an alveolar macrophage delivery system of ofloxacin via pulmonary inhalation. *Int J Pharm*. 2013;441(1–2):562–569.
21. Hwang SM, Kim DD, Chung SJ, Shim CK. Delivery of ofloxacin to the lung and alveolar macrophages via hyaluronan microspheres for the treatment of tuberculosis. *J Control Release*. 2008;129(2):100–106.
22. Palazzo F, Giovagnoli S, Schoubben A, Blasi P, Rossi C, Ricci M. Development of a spray-drying method for the formulation of respirable microparticles containing ofloxacin-palladium complex. *Int J Pharm*. 2013;440(2):273–282.
23. Chimote G, Banerjee R. Evaluation of antitubercular drug-loaded surfactants as inhalable drug-delivery systems for pulmonary tuberculosis. *J Biomed Mater Res A*. 2009;89(2):281–292.

24. Ganguly S, Moolchandani V, Roche JA, et al. Phospholipid-induced in vivo particle migration to enhance pulmonary deposition. *J Aerosol Med Pulm Drug Deliv*. 2008;21(4):343–350.
25. Mansour H, Wang DS, Chen CS, Zografi G. Comparison of bilayer and monolayer properties and phospholipid systems containing dipalmitoylphosphatidyglycerol and dipalmitoylphosphatidylinositol. *Langmuir*. 2001;17(21):6622–6632.
26. Mansour HM, Zografi G. Relationships between equilibrium spreading pressure and phase equilibria of phospholipid bilayers and monolayers at the air–water interface. *Langmuir*. 2007;23(7):3809–3819.
27. Mansour HM, Zografi G. The relationship between water vapor absorption and desorption by phospholipids and bilayer phase transitions. *J Pharm Sci*. 2007;96(2):377–396.
28. Hickey AJ, Mansour HM. Formulation challenges of powders for the delivery of small molecular weight molecules as aerosols. In: Rathbone MJ, editor. *Modified-Release Drug Delivery Technology*. New York, NY: Informa Healthcare; 2008:573–602.
29. Hickey AJ, Mansour HM. Delivery of drugs by the pulmonary route. In: Florence AT, Siepmann J, editors. *Modern Pharmaceutics*. New York, NY: Taylor and Francis; 2009:191–219.
30. Hickey AJ, Mansour HM, Telko MJ, et al. Physical characterization of component particles included in dry powder inhalers. I. Strategy review and static characteristics. *J Pharm Sci*. 2007;96(5):1282–1301.
31. Hickey AJ, Mansour HM, Telko MJ, et al. Physical characterization of component particles included in dry powder inhalers. II. Dynamic characteristics. *J Pharm Sci*. 2007;96(5):1302–1319.
32. Suarez S, Hickey AJ. Drug properties affecting aerosol behavior. *Respir Care*. 2000;45(6):652–666.
33. Wu X, Li X, Mansour HM. Surface analytical techniques in solid-state particle characterization: implications for predicting performance in dry powder inhalers. *KONA Powder and Particle Journal*. 2010;28:3–19.
34. Xu Z, Mansour HM, Hickey AJ. Particle interactions in dry powder inhaler unit processes. *Journal of Adhesion Science and Technology: Special Issue on Adhesion Aspects in Pharmaceutical Sciences*. 2011;25(4–5):451–482.
35. Xu Z, Mansour HM, Mulder T, McLean R, Langridge J, Hickey AJ. Heterogeneous particle deaggregation and its implication for therapeutic aerosol performance. *J Pharm Sci*. 2010;99(8):3442–3461.
36. Adi H, Traini D, Chan HK, Young PM. The influence of drug morphology on aerosolisation efficiency of dry powder inhaler formulations. *J Pharm Sci*. 2008;97(7):2780–2788.
37. Dunbar CA, Hickey AJ, Holzner P. Dispersion and characterization of pharmaceutical dry powder aerosols. *KONA Powder and Particle Journal*. 1998;16:7–45.
38. Zeng XM, Martin GP, Marriott C. *Particulate Interactions in Dry Powder Formulation for Inhalation (Pharmaceutical Science Series)*. London, UK: Taylor and Francis; 2001.
39. Wu X, Zhang W, Hayes D Jr, Mansour HM. Physicochemical characterization and aerosol dispersion performance of organic solution advanced spray-dried cyclosporine A multifunctional particles for dry powder inhalation aerosol delivery. *Int J Nanomedicine*. 2013;8:1269–1283.
40. Wu X, Hayes D Jr, Zwischenberger JB, Kuhn RJ, Mansour HM. Design and physicochemical characterization of advanced spray-dried tacrolimus multifunctional particles for inhalation. *Drug Des Devel Ther*. 2013;7:59–72.
41. Meenach SA, Vogt FG, Anderson KW, Hilt JZ, McGarry RC, Mansour HM. Design, physicochemical characterization, and optimization of organic solution advanced spray-dried inhalable dipalmitoylphosphatidylcholine (DPPC) and dipalmitoylphosphatidylethanolamine poly(ethylene glycol) (DPPE-PEG) microparticles and nanoparticles for targeted respiratory nanomedicine delivery as dry powder inhalation aerosols. *Int J Nanomedicine*. 2013;8:275–293.
42. Li X, Mansour HM. Physicochemical characterization and water vapor sorption of organic solution advanced spray-dried inhalable trehalose microparticles and nanoparticles for targeted dry powder pulmonary inhalation delivery. *AAPS PharmSciTech*. 2011;12(4):1420–1430.
43. Li X, Hayes D, Mansour HM. Targeted lung delivery by inhalable multifunctional microparticulate/nanoparticulate aerosols for cystic fibrosis combination drug/mucolytic treatment. *Pediatr Pulmonol*. 2011;346–346.
44. Park CW, Rhee YS, Vogt FG, et al. Advances in microscopy and complementary imaging techniques to assess the fate of drugs ex vivo in respiratory drug delivery: an invited paper. *Adv Drug Deliv Rev*. 2012;64(4):344–356.
45. Mansour HM, Hickey AJ. Raman characterization and chemical imaging of biocolloidal self-assemblies, drug delivery systems, and pulmonary inhalation aerosols: a review. *AAPS PharmSciTech*. 2007;8(4):E99.
46. Aerosols, nasal sprays, metered-dose inhalers, and dry powder inhalers monograph. In: *USP 29-NF 24: United States Pharmacopoeia and the National Formulary: The Official Compendia of Standards*. Vol 29/24. Rockville, MD: United States Pharmacopeial Convention; 2006:2617–2636.
47. Finlay WH. *The Mechanics of Inhaled Pharmaceutical Aerosols: An Introduction*. London, UK: Academic Press; 2001.
48. Finlay W [webpage on the Internet]. ARLA respiratory deposition calculator. Edmonton, AB: Aerosol Research Lab of Alberta; 2008. Available from: http://www.mece.ualberta.ca/arla/impactor_mmad_calculator.html. Accessed June 20, 2010.
49. Brittain HG. X-ray diffraction III: pharmaceutical applications. *Spectroscopy*. 2001;16:7.
50. Alves GP, Santana MHA. Phospholipid dry powders produced by spray drying processing: structural, thermodynamic and physical properties. *Powder Technology*. 2004;145(2):139–148.